

REPORT DOCUMENTATION PAGE

Form Approved
OMB No. 0704-0188

Public reporting burden for this collection of information is estimated to average 1 hour per response, including the time for reviewing instructions, searching existing data sources, gathering and maintaining the data needed, and completing and reviewing this collection of information. Send comments regarding this burden estimate or any other aspect of this collection of information, including suggestions for reducing this burden to Department of Defense, Washington Headquarters Services, Directorate for Information Operations and Reports (0704-0188), 1215 Jefferson Davis Highway, Suite 1204, Arlington, VA 22202-4302. Respondents should be aware that notwithstanding any other provision of law, no person shall be subject to any penalty for failing to comply with a collection of information if it does not display a currently valid OMB control number. PLEASE DO NOT RETURN YOUR FORM TO THE ABOVE ADDRESS.

1. REPORT DATE (DD-MM-YYYY)

2. REPORT TYPE

Technical Papers

3. DATES COVERED (From - To)

4. TITLE AND SUBTITLE

5a. CONTRACT NUMBER

5b. GRANT NUMBER

5c. PROGRAM ELEMENT NUMBER

6. AUTHOR(S)

5d. PROJECT NUMBER

2308
5e. TASK NUMBER

M13C
5f. WORK UNIT NUMBER

346057

7. PERFORMING ORGANIZATION NAME(S) AND ADDRESS(ES)

Air Force Research Laboratory (AFMC)
AFRL/PRS
5 Pollux Drive
Edwards AFB CA 93524-7048

8. PERFORMING ORGANIZATION REPORT

9. SPONSORING / MONITORING AGENCY NAME(S) AND ADDRESS(ES)

Air Force Research Laboratory (AFMC)
AFRL/PRS
5 Pollux Drive
Edwards AFB CA 93524-7048

10. SPONSOR/MONITOR'S ACRONYM(S)

11. SPONSOR/MONITOR'S NUMBER(S)

Please see attached

12. DISTRIBUTION / AVAILABILITY STATEMENT

Approved for public release; distribution unlimited.

13. SUPPLEMENTARY NOTES

14. ABSTRACT

20030116 061

15. SUBJECT TERMS

16. SECURITY CLASSIFICATION OF:

a. REPORT

Unclassified

b. ABSTRACT

Unclassified

c. THIS PAGE

Unclassified

17. LIMITATION OF ABSTRACT

A

18. NUMBER OF PAGES

19a. NAME OF RESPONSIBLE PERSON

Leilani Richardson

19b. TELEPHONE NUMBER

(include area code)
(661) 275-5015

2308M13C

MEMORANDUM FOR PRS (Contractor/In-House Publication)

FROM: PROI (TI) (STINFO)

16 August 1999

SUBJECT: Authorization for Release of Technical Information, Control Number: AFRL-PR-ED-TP-FY99-0163
Strakey and Talley, "Phase Doppler Interferometry with Probe-to-Droplet Size Ratios Less than Unity.
Part I: Trajectory Errors"

✓ DTS

Journal submission

(Statement A)

1. This request has been reviewed by the Foreign Disclosure Office for: a.) appropriateness of distribution

Phase Doppler Interferometry with Probe-to-Droplet Size Ratios Less Than Unity

Part I: Trajectory Errors

P. A. Strakey* & D. G. Talley

Air Force Research Laboratory, AFRL/PRSA, 10. E. Saturn Blvd., Edwards AFB, CA 93524

S. V. Sankar & W. D. Bachalo

Consultants, 14660 Saltamontes Way, Los Altos Hills, CA 94022

Abstract

Phase Doppler interferometry utilizing a probe volume much smaller than the droplets being measured has been shown to work well when coupled with a phase ratio and intensity validation scheme which is capable of eliminating trajectory dependent scattering errors. Ray-tracing and geometric optics models were used to quantitatively demonstrate the type and magnitude of trajectory errors through stochastic trajectory calculations. Measurements with mono-dispersed water droplet streams and glass beads have been performed to validate the model calculations and to characterize the probe volume. Scattered light intensity has also been shown to provide a robust means of determining the probe cross-sectional area which is critical for making accurate mass flux measurements.

Introduction

Measurements of particle size, velocity and volume flux in optically dense sprays is an emerging and challenging field. One of the most promising techniques for making these measurements is phase Doppler interferometry. The phase Doppler technique, which works well in low number density sprays (N less than 10^3 cm^{-3}) in the size range of 5-300 μm , is fraught with problems in dense sprays where the number densities can reach 10^5 cm^{-3} in the same size range. The Phase Doppler Particle Analyzer (PDPA) is a single particle counter which relies on the fact that there is no more than one particle in the probe volume at any given time. It is unclear how the instrument responds when several particles are simultaneously present in the probe volume. Sankar *et al.* have shown that the Doppler Signal Analyzer (DSA) can, in some instances, measure one of two particles simultaneously present in the probe volume [1]. The DSA cannot, however, account for the other particle(s) present in the probe volume. The result can be a severe underestimation in the particle number density and volume flux, and a potential biasing in the particle size distribution.

High pressure liquid rocket injectors produce a wide range of droplet sizes depending on the injector flow-rates, chamber pressure and injector geometry (shear coaxial, swirl, impinging, etc.). In an effort to maintain high engine operating efficiency, liquid rocket injectors usually operate at very high flow-rates, on the order of several kilograms per second, and high back-pressure. This combination of high flow-rate and high pressure results in high number densities of relatively large droplets. A shear coaxial injector currently being studied at AFRL using water and nitrogen as simulants for LOX and GH_2 , has produced droplet sizes in the range of 2 - 200 μm with peak number densities of about 10^5 cm^{-3} . The conventional phase Doppler technique requires that the diameter of the probe volume be at least twice as large as the largest droplet size to be measured. This rule of thumb is designed to minimize trajectory dependent scattering errors which occur when the droplet size becomes larger than the probe radius. The probe volume can be estimated by;

$$V = \frac{\pi D_w^2 \cdot D_s}{4 \cdot \sin(\theta)} \quad (1)$$

* To whom correspondence should be addressed

where D_w is the $1/e^2$ beam waist diameter, D_s is the apparent slit width and θ is the angle of the receiver with respect to the laser beams. The apparent slit width is equal to the slit width multiplied by the magnification factor of the receiving optics. For a scattering angle of 30° , a beam waist of $400 \mu\text{m}$ and an apparent slit width of $200 \mu\text{m}$, the probe volume is $5.0 \times 10^{-5} \text{cm}^3$. The probability of finding n particles within the probe volume can be determined by;

$$P(n) = \frac{(VN)^n}{n!} e^{-(VN)} \quad (2)$$

where V is the probe volume, and N is the particle number density [1]. For the above listed configuration with $N=10^5$ droplets/cm³, the ratio, $P(2)/P(1)=2.5$, which means that probability of finding two particles in the probe volume is two and a half times the probability of finding one particle in the probe volume. Since scattered light intensity from a droplet is proportional to the droplet diameter squared, and the intensity distribution of the probe beams is Gaussian, the probe size for a given minimum signal detectability increases with increasing droplet size. In Eq. 1, the diameter of the probe volume is estimated to be D_w , which could better be described as an average probe volume diameter.

There is a relatively small collection of published literature with respect to making phase Doppler measurements when the probe to particle diameter ratio is small ($D_w/D < 1.0$) [2-6]. Most of these studies are theoretical in nature involving geometric optics or generalized Lorentz-Mie theory to calculate the far-field scattering for droplets comparable to or larger than the probe diameter. One particular problem has been referred to as trajectory dependent scattering errors or trajectory ambiguities [2-17]. Hadalupas and Liu [2] presented a theoretical study using a geometric optics phase Doppler response model to predict the resulting phase and intensity for various droplet trajectories through the probe volume for D_w/D ratios down to 0.35. They showed, for non-absorbing droplets at various scattering angles, that significant sizing errors can occur for certain trajectories on the edge of the probe volume away from the receiver. They concluded that most of the sizing errors can be eliminated by an appropriate phase and intensity validation scheme. They also showed that forward scattering is preferable to side or backward scattering with respect to minimizing trajectory errors when sizing non-absorbing droplets.

Haugen and co-workers [3] demonstrated in theory and through experimentation with a mono-dispersed droplet stream that trajectory errors can be eliminated with a three detector system for a D_w/D ratio of 0.17 using a phase ratio criteria between the two pairs of detectors. The technique was shown to work best when the detector separation ratio between detectors 1-2 and detectors 1-3 was a non-integer number with a fractional part close to 0.5, i.e., $S_{13}/S_{12} = 2.5$ or 3.5. The use of non-integer detector separations will be discussed later.

Hadalupas and Taylor [4] have also proposed a phase validation criteria to eliminate sizing errors due to trajectory ambiguity, but their method requires that the maximum droplet size in a spray be known *a priori*, and that the optical system be arranged such that the maximum measured phase due to refraction be less than the minimum phase due to reflection over the size range of interest. This method would be difficult to apply to a spray in which the investigator has no knowledge about the anticipated droplet size range.

Various researchers have proposed variations on the standard phase Doppler technique, which are designed to reduce or eliminate sizing errors. These techniques involve changing the receiving optics orientation with respect to the predominant flow direction as well as adding additional receiving optics. A review of these techniques and a discussion of some of the problems of the variations on the standard phase Doppler technique was presented by Sankar and Bachalo [14]. Their conclusion was that all of the variations on the standard PDI technique introduced new problems that would have to be overcome to make any of the techniques feasible.

Sankar *et al.* [15] have also demonstrated through geometric optics modeling and experimentation that significant sizing errors occur for certain droplet trajectories for D_w/D ratios less than about 2.9. They demonstrated that trajectory errors can be minimized by increasing the laser beam intersection angle. Their experimental results have shown this to work quite well for D_w/D ratios down to 1.4.

Sankar and coworkers [16] have also demonstrated that trajectory errors occur for droplet trajectories along the edge of the probe volume and are associated with a low scattering intensity, which can subsequently be used to identify and eliminate these erroneous measurements. There is no fundamental limit on the minimum D_w/D ratio for which

this technique would work. Intensity validation is an attractive technique because most existing PDI systems already have the capability to measure peak scattering intensity and to reject measurements below a preset scattering intensity.

Trajectory Errors

One of the problems associated with reducing the size of the probe volume is trajectory dependent scattering which is a result of the Gaussian nature of the laser beam waist and occurs when the droplet-to-probe diameter ratio, D_w/D , is less than approximately 2.9 [5]. Droplets of this size which pass through the edge of the probe volume, as shown in Figure 1, have a significant reflection scattering component which can result in the particle being erroneously sized as either a smaller or larger droplet depending on the optical configuration and droplet size. This phenomenon has been previously demonstrated with both theoretical light scattering calculations and experimentation [16]. It has also been shown that these reflection tainted trajectories can be identified by their relatively low light scattering intensity [16].

One of the goals of this investigation is to demonstrate with both theoretical calculations and experimentation, that trajectory dependent errors can be eliminated with an appropriate phase ratio and intensity validation scheme. The ability to eliminate trajectory dependent scattering errors allows for making the beam waist diameter and hence probe volume much smaller than the largest droplet size to be measured, thereby allowing the application of phase Doppler interferometry in sprays with significantly higher number densities than has previously been possible.

Modeling and Experimental Results and Discussion

Geometric Optics Modeling

A previously developed phase Doppler response model [7] was used to study the effect of droplet trajectory on phase response and scattering intensity. The model is a geometric optics based scattering model that accounts for the Gaussian nature of the illuminating probe beams by integrating the appropriate scattering functions over the surface of the receiving lens. The model accounts for external surface reflection ($p=0$), refraction ($p=1$), and the first four modes of internal reflection ($p=2$ to $p=5$). The model calculates the resulting phase and intensity for each detector in the receiver. The geometric optics model has been shown to yield excellent agreement with Lorentz-Mie theory for droplet sizes larger than the wavelength of light when the scattered phase and intensity are integrated over a typical ($f5.0$) receiver lens [14]. The model will not be discussed further here while the reader is referred to the published description of the model [7].

A schematic of the optical orientation is presented in Figure 2. The receiver lies in the x - y scattering plane at 30° with respect to the beam propagation direction. The trajectory coordinate, η , is defined as y'/D_w , where y' is the distance from the center of the probe volume in the scattering plane normal to the beam propagation direction and D_w is the $1/e^2$ beam waist diameter. For the calculations presented here, all trajectories were normal to the scattering plane in the negative z direction. Negative values of η would correspond to trajectories on the side of the probe farthest from the receiver. The calculations were performed for the optical configuration listed under case 1 in Table 1. Figure 3 contains plots of calculated scattered light intensity normalized by the maximum intensity, calculated droplet diameter normalized by the actual diameter and the calculated phase ratio between detector pairs 1-3 and 1-2 normalized by the detector separation ratio (2.96). These calculations are shown as a function of the droplet trajectory coordinate, η , for water droplet diameters of 60 μm , 100 μm and 200 μm . In these plots the calculated diameter is based on the phase response of detector pairs 1-3. Since the instrument is only capable of measuring positive phase values, the calculated phase values are subsequently reported as being positive. For example, a 60 μm droplet at $\eta = -2.0$, results in a phase value of $\phi_{12} = -81^\circ$, and $\phi_{13} = -260^\circ$ due to reflection dominated scattered light. The instrument actually measures ϕ_{12} as $-81^\circ + 360^\circ = 279^\circ$. Similarly, $\phi_{13} = -260^\circ + 360^\circ = 100^\circ$. Since ϕ_{13} is actually multi-valued over the detectable size range the correct ϕ_{13} is calculated by using ϕ_{12} to determine which "cycle" ϕ_{13} is in. ϕ_{13} is calculated according to Equation 3;

$$\phi_{13} = \phi_{13} + \text{Trunc} \left[\frac{\phi_{12} \cdot S_{13}}{S_{12} \cdot 360^\circ} \right] \cdot 360^\circ \quad (3)$$

where *Trunc* is a truncation function equal to the integer portion of the division.

For a 60 μm droplet (Figure 3a), for η greater than -0.3, refraction dominates the scattered light signal and the normalized diameter and phase ratio are equal to 1.0. For η less than -0.3, reflection begins to contribute significantly to the scattered light signal resulting in a measured diameter of 240 μm which is much larger than the actual diameter of 60 μm . It is also interesting to note that the normalized phase ratio in this region is still equal to one indicating that most of these measurements would pass the phase ratio validation criteria which requires that $\phi_{13}/\phi_{12} = S_{13}/S_{12}$ within a tolerance band of +/- 10%. This is a problem unique to instruments with a detector separation ratio equal to an integer number. For such a detector configuration, any reflectively dominated trajectory will pass the phase ratio validation criteria. For instance, for a 60 μm droplet at $\eta = -1.0$, ϕ_{12} is calculated to be $\angle 81.7^\circ$ and $\phi_{13} = -260.0^\circ$. The instrument would measure ϕ_{12} as $-81.7^\circ + 360.0^\circ = 278.3^\circ$. Similarly $\phi_{13} = \angle 260.0^\circ + 360.0^\circ = 100.0^\circ$. Using Equation 3, ϕ_{13} is found to be in the third cycle, therefore $\phi_{13} = 100.0^\circ + 720.0^\circ = 820.0^\circ$. The resulting phase ratio, $\phi_{13}/\phi_{12} = 2.95$ which is almost exactly equal to the detector separation ratio S_{13}/S_{12} of 2.96.

This has been demonstrated in theory before and can be overcome by using a non-integer detector separation ratio such as 2.5 [3]. Also in Figure 3a, note that the normalized phase ratio in the region of $-0.6 < \eta < -0.2$ is not equal to 1.0 and would probably be rejected by the instrument, even with an integer detector separation ratio. The scattered light for these trajectories is a mix of refraction and reflection and thus, the phase is a complicated result of the coherent interaction between these two scattering modes resulting in phase ratios deviating from 1.0.

Figures 3b and 3c show similar results for 100 μm and 200 μm droplets, respectively. Figure 3c shows that for a 200 μm droplet the refractively dominated scattered light has a peak intensity around $\eta = 1.0$, whereas the reflectively dominated light is centered at approximately $\eta = -1.5$. This is because refraction and reflection originate from opposite sides of the droplet as illustrated in Figure 2. For the 200 μm droplets (Fig. 3c) note that the normalized phase ratio and normalized calculated droplet size does deviate from one throughout the beam waist. This is due to the decrease in signal visibility of the refracted light signal for the larger droplet size. The signal visibility is defined as the relative amplitude modulation of the scattered light signal as a droplet passes through the probe volume.

Figures 3a-3c shows that severe sizing errors can occur for certain trajectories through the probe volume and that most of these erroneous measurements will pass the phase ratio validation criteria of a three detector instrument when the detector separation ratio is close to an integer number. Figure 3 does not, however, reveal the magnitude of the problem, which is dependent on the relative probability of any given trajectory and the minimum detectable signal that will trigger the burst detector. Also, another type of measurement error sometimes referred to as the "slit effect", can cause erroneous measurements [17]. The slit effect occurs for certain particle trajectories when the spatial filter in the receiving optics, referred to as the slit, blocks the refractively scattered light signal but passes the reflectively scattered light signal, resulting in a measurement error similar to that shown in Figure 3. Figure 4 illustrates the slit effect.

Stochastic Ray-Trace Modeling

In order to investigate the combined effects of trajectory error and slit effect, a ray tracing algorithm was used to predict the relative intensity of refractively and reflectively scattered light as a function of droplet size and trajectory in a two-dimensional probe volume defined by the beam waist and receiver slit. Droplet trajectories, as defined by the x and y coordinates were chosen by a random number generator and encompassed an area much larger than the beam waist and slit width. The resulting scattered light intensity was calculated and compared to a minimum detectable signal level.

The minimum detectable raw signal for the Aerometrics DSA was determined to be 1 mv by experimentation at a threshold setting of 3 mv using a 16 point Fourier transform burst detector. The threshold setting is the minimum amplitude of the high-pass filtered, log amplified signal before triggering can occur. A setting of 3 mv is close to the minimum useable level before triggering on background noise can occur.

For the droplets with calculated scattered light intensities greater than the minimum detectable intensity, significant sizing errors were determined to occur when the intensity of the reflectively scattered light component was greater than 50% of the total scattered light intensity. This criteria was determined through geometric optics calculations similar to those in Fig. 3. This type of ray-tracing calculation can determine which trajectories will result in sizing errors, but provides no information as to the magnitude of the errors. For each droplet size and optical configuration 25,000 random trajectories were selected and the fraction of measurements dominated by reflective contributions were tabulated. Figure 5 shows the fraction of measurements in which sizing errors would occur. Calculations were performed for beam waist diameters of 60 μm and 300 μm with and without the receiver slit in place. For the 300 μm probe diameter the relative number of erroneous measurements increases with droplet size and also increases when the receiver slit is accounted for. The 60 μm beam diameter reveals an increase in erroneous measurements, in comparison to the 300 μm probe, for any given droplet size. This is due to an increased reflective contribution to the scattered light signals for the larger droplet size to beam waist ratio. With the 60 μm beam waist, there appears to be no effect of the receiver slit. In other words, the same errors would occur even without the slit blocking the refractively scattered light for certain trajectories. The reason for this is that with a beam waist smaller than the apparent slit width, errors occur only for droplet trajectories on the far side of the beam waist with respect to the receiver. For these trajectories, sizing errors occur as a result of the Gaussian intensity distribution of the probe beams and the introduction of the receiver slit does not serve to further aggravate this problem.

Figure 5 shows that an alarming number of sizing errors can occur for droplet sizes much larger than the beam waist. For dense spray applications, when the beam waist is made much smaller than the largest droplets being measured, the largest number of trajectory errors will occur in the droplet size classes with the highest number density. For a beam waist of 60 μm and a maximum droplet size of about 300 μm , peak number densities in a typical dense spray might occur in the 50-100 μm range. It is these droplets, being erroneously measured as much larger droplets, which will statistically contribute the most to errors in the higher moment diameters such as D_{30} or D_{32} and in the measured mass flux, which tends to scale with D_{30} .

Stochastic Geometric Optics Modeling and Experimentation

Small Droplets Being Measured as Larger Droplets

Knowing that the receiver slit does not contribute to sizing errors for beam waists smaller than the apparent slit width, we can now use the geometric optics model, which does not account for slit effects, to more quantitatively estimate the magnitude of trajectory dependent scattering errors. An approach similar to that described above for the ray-tracing calculations was taken. A random number generator randomly selected trajectories (with respect to the y' direction) normal to the scattering plane and the resulting phase and intensity were calculated. Negative phases were then calculated as being positive and droplet sizes were calculated using a linear refractive phase response curve. The calculated droplet sizes were grouped in size bins to yield a histogram of counts versus droplet size similar to the way that the Aerometrics PDI instrument works experimentally. All calculation and experiments were performed with water droplets with a refractive index of 1.33-0.0i. The optical configuration was the same as in case 1 of Table 1.

To quantitatively verify the model calculations, several experiments were conducted using an acoustically driven mono-dispersed droplet generator. A laminar stream of water issuing from a small orifice was perturbed by a piezoelectric crystal mounted on the droplet generator. This resulted in a steady stream of droplets traveling at 13 m/s at a rate of about 10^4 droplets per second. For each droplet size studied, 30,000 data points were collected while the droplet generator was traversed, by hand, throughout the probe volume over a period of about 30 seconds. The manual traversing produced pseudo-random trajectories through the probe volume. In an effort to verify the randomness of the trajectories, each 30,000 point data set was repeated a total of three times and the Sauter mean diameter, D_{32} , for each run was calculated. The standard deviation normalized by the mean D_{32} , for the three runs was on the order of 11% for each droplet size studied. Although there was some variation from run to run, each data set does represent a random selection of trajectories fairly well.

The PDPA used in this study was a standard 2-component, fiber optically coupled, DSA based system manufactured by Aerometrics Inc. The transmitter produced a beam waist of 352 μm with a 500 mm focusing lens. In order to reduce the beam waist diameter, a beam expander was constructed using a negative achromatic lenses ($f_1 = -12$ mm)

and a positive achromatic lens ($f_2=60$ mm) to expand and re-collimate the beams inside of the transmitter from an initial diameter of 2 mm to a final diameter of 10.0 mm. The resulting beam waist was characterized by placing a microscope objective at the beam crossover point and projecting the beam waist onto a rotating white target. The rotation of the target served to reduce the speckle pattern formed by the coherent laser. The beam waist was then imaged with a CCD camera and recorded with a frame grabber. The $1/e^2$ beam waist, which was closely Gaussian in shape was measured to be 60 μm in diameter. The standard receiver slit, which was 100 μm was replaced with a 50 μm slit in order to further reduce the probe volume. Due to the factor of two magnification in the receiving optics, the apparent slit width was 100 μm .

Figure 6 contains a series of histograms of calculated diameter from the geometric optics model, and measured diameter from the mono-dispersed droplet experiments, for random trajectories through the probe volume for a droplet diameter of 57 μm . The optical configuration was that of case 1 of Table 1. The top series of plots, Fig. 6a, shows the model and experimental results without the use of a phase ratio criteria. The model shows excellent agreement with the experimental results not only for the location of the erroneous peak in the histograms, which occurs at 250 μm , but also in the relative number of trajectory errors in comparison to the correctly measured droplets at 57 μm . For the experimental histogram in Fig. 6a, the measured D_{32} was 224 μm , which was dominated by the relatively few falsely measured large droplets. This tremendous measurement error demonstrates the need to reject the trajectory dependent errors.

Figure 6b contains histograms of the same data set presented in Fig. 8a, but with the phase ratio criteria applied. The phase ratio criteria requires that $(\varphi_{13}/\varphi_{12}) = (S_{13}/S_{12})$ to within $\pm 10\%$. Both the model calculations and the experimental data confirm that almost all of the erroneous measurements pass the phase ratio validation criteria, which is a result of the near integer detector separation ratio, S_{13}/S_{12} of 2.96.

Figure 6c, shows the same data set as Fig. 8b, after a 10:1 intensity validation criteria is applied. The 10:1 intensity validation scheme rejects measurements with a scattering intensity less than $1/10^{\text{th}}$ the maximum scattering intensity in each size class. Both the model and experiment show that all of the erroneous measurements are rejected.

Figures 7a-c show model calculations and experimental results for a droplet diameter of 98 μm . The data is again presented without the phase ratio validation criteria (Fig. 7a), with the phase ratio criteria applied (Fig. 7b) and with the 10:1 intensity validation criteria applied (Fig. 7c). The results are the same as for the 57 μm droplets confirming that the phase ratio criteria accepts most of the erroneous measurements at 200 μm , but that all of these can be rejected with a 10:1 intensity validation criteria.

Model calculations were performed over a wide range of droplet sizes between 10 and 350 μm in diameter. The model has shown that significant sizing errors occur for D_w/D ratios less than about 5.0 for the optical configuration of case 1, Table 1. Due to minimum detectability limits of the instrument, the practical maximum D_w/D at which sizing errors occur would be about 2.0. The model has also shown that a 10:1 intensity validation criteria is sufficient to reject any trajectory dependent scattering error resulting in a droplet showing up as a larger droplet. In most sprays, this will be the statistically dominant sizing error. Large droplets passing along the far side of the probe volume can, however, be misinterpreted as smaller droplets with corresponding low scattering intensity. The intensity validation criteria will not be able to reject these types of errors.

Large Droplets Being Measured as Smaller Droplets

In order to reject errors associated with large droplets being measured as much smaller droplets, a phase ratio validation criteria can be applied using a non-integer detector separation as demonstrated by Haugen *et al* [3]. In theory, a non-integer phase validation criteria should also be able to reject small droplets showing up as much larger droplets. An experiment was conducted in which the detector separations, S_{12} and S_{13} were changed by placing a mask in front of the receiver lens, effectively blocking off some portion of each detector. This resulted in a separation of detectors 1 and 2 of 25.0 mm and a separation of detectors 1 and 3 of 65.0 mm (case 2, Table 1). The detector separation ratio was 2.6. Experiments were repeated with the pseudo-random mono-dispersed droplet stream for droplet diameters of 61 μm , 102 μm and 250 μm .

Figure 8 contains histograms for the 250 μm droplet size. For this relatively large droplet size, a reflective error results in the droplet being measured as a much smaller droplet of 60 μm in diameter. The broadness of the two peaks in Fig. 8a is a result of some degree of non-sphericity for the relatively large droplet size of 250 μm . This was verified by imaging the droplet stream with a CCD camera a strobelight. Applying the phase ratio criteria of $\pm 10\%$ to the data in Fig. 8a results in the histogram shown in Fig. 8b, which shows a tremendous decrease in the number of erroneous measurements at the 60 μm peak. There are, however some errors that pass the validation criteria, but statistically, the overall error in a typical spray would be very small, because the number density of "real" droplets in the 60 μm size range would be much larger than the number density at 250 μm .

For the experiments with the 61 μm droplets, the number of counts at the "reflection peaks" at 70 μm and 270 μm were reduced by a factor of almost eight with the non-integer detector separation and phase ratio validation criteria of $\pm 10\%$, but enough passed the criteria to produce a D_{32} of 101 μm . Figure 9 shows the volume distribution, which is the number of counts multiplied by D^3 for each size class, with and without the phase ratio validation criteria. The volume distributions are used to illustrate the significant effect of a very small number of very large droplets. Similar results were obtained with the 102 μm droplets. The small number of measurements that pass the phase ratio validation criteria could be the result of some small amount of noise related error in the phase measurement due to the relatively short transit times.

Both the calculations and experiments indicate that trajectory dependent phase errors only occur at scattering intensities well below a scattering intensity that is one tenth of the maximum intensity for each droplet size. Similar results have been published previously and demonstrate that probe diameters much smaller than the droplets being measured can provide accurate droplet size measurements when phase ratio with a non-integer detector separation ratio and scattering intensity are used as criteria to reject trajectory dependent scattering errors.

Detailed Probe Volume Characterization

The model calculations and experimental results presented herein have shown that even for a beam waist much smaller than the droplet being measured, accurate size measurements can be made within a 10:1 intensity range. These results do not, however, necessarily show that droplets within the 10:1 intensity range are being validated by the instrument. Also, the effective size of the probe cross-sectional area, which can be ascertained by the measured scattered light intensity has not been shown to be necessarily accurate. For a Gaussian beam waist, the probe cross-sectional area is a function of the beam waist diameter at the 10:1 lower intensity cutoff and the apparent slit width and scattering angle according to Equation 4.

$$A = \frac{D_{w10\%} \cdot D_s}{\sin(\theta)} \quad (4)$$

In order to characterize the probe volume, it was necessary to traverse the probe volume, both in the x and y direction with a stream of droplets in which the absolute droplet positions within the probe volume were known. It was determined that several hours of data collection would be required to completely map the probe volume and the mono-dispersed droplet generator was not capable of maintaining a sufficiently steady stream of droplets for this period of time. It was found that a similar type of experiment could be conducted using a glass bead mounted on 126 μm steel wire which was in turn mounted on a rotating disk. The rotating disk would "swing" the glass bead through the probe volume at a velocity of 16 m/s. This arrangement was found to produce very steady and repeatable results. The glass bead was examined under a microscope to insure that it was free from surface defects and inclusions. Glass has a refractive index of 1.51 in air, which yielded a maximum measurable size of 370 μm with the optical configuration listed in Table 1, case 1.

The setup was mounted on a three-dimensional translating stage which allowed the bead to be traversed through the probe volume with a positioning accuracy of 1 μm . The bead was traversed in the x direction, towards the receiver at 20 μm steps, while 300 measurements were collected at each spatial location. The bead was then traversed along the direction of the beams at 50 μm steps. The resulting data provided a two-dimensional map of measured bead

size, scattering intensity and validation rate across the entire probe cross-sectional area. Each data set, which was comprised of approximately 120 data points, was interpolated to allow contour plots to be presented.

Figure 10 contains contour plots of the log of the intensity, the intensity within a 10:1 range, the measured D_{10} , and the instrument validation rate. In the plots the beams are originating from the upper left hand corner of the plots and the receiver is located to the right of the plot. The coordinate positions are relative to the initial bead starting position. Data is shown everywhere that an instrument trigger was obtained. Figure 10a shows the logarithm of the normalized intensity distribution for a 330 μm glass bead. The intensity was normalized by the maximum scattering intensity. Note the "island" of reflectively scattered light centered at $x = 530 \mu\text{m}$ which is a factor of 40 less intense than the refractively scattered light. The two scattered light modes are separated in space due to the fact that the refractively scattered light and reflectively scattered light originate from opposite sides of the bead. For the large bead size studied here, there are trajectories between the two modes ($p=0$ and $p=1$) which result in no detectable light reaching the receiver. These results agree very well with the model which shows that the reflectively scattering trajectories are completely separated spatially from the refractive trajectories for large droplets. Also shown in Figure 10a is the assumed probe volume (parallelogram) which is 64 μm in width with a 100 μm apparent slit length. Without an intensity-based validation criteria, the effective probe cross-sectional area, as determined by instrument triggering, would be much greater than the assumed area.

Figure 10b shows the linear normalized intensity distribution over a 10:1 intensity range. Normal to the beam propagation direction, the measured beam diameter is very close to the assumed diameter of 64 μm . The length of the probe volume (in the y direction) as defined by a 10:1 intensity range was found to be about 125 μm . The fact that the measured slit width is larger than the physical slit width of 100 μm can be attributed to the finite interrogation spot size on the droplet surface which yields an average scattering intensity over this region. The effective slit width is also increased by the resolution of the receiving optics which has a blur spot of 15 μm . The blur spot and the finite interrogation spot size tend to spread the intensity distribution over a larger area.

Figure 10c is a contour plot of the measured D_{10} normalized by the actual bead diameter of 330 μm . Also shown is the probe volume as defined by a 10:1 intensity validation criteria. Within the probe volume, the measured D_{10} is very close to the actual bead diameter. Outside of the 10:1 probe volume significant sizing errors occur with the 330 μm glass beam being measured as small as 20 μm for certain trajectories. Figure 10d shows the validation rate normalized by the maximum or "ideal" validation rate of 100%. Within the 10:1 probe volume, the validation rates are very close to 100 %, except at the edges where the validation rates begin to drop off with most of the rejections being due either to the phase ratio criteria or due to the bead being measured as a diameter outside the measurable range.

These measurements show that even for a bead diameter 5.5 times larger than the $1/e^2$ beam diameter, accurate sizing is possible within a 10:1 intensity range. The diameter of the probe as defined by a scattering intensity $1/10^{\text{th}}$ the maximum intensity is very close to the assumed diameter of 64 μm . The effective apparent slit width was found to be about 25% larger than the assumed width, which could easily be accounted for by assuming a larger slit width.

Similar results were also obtained with a 100 μm glass bead which showed that the effective slit width within the 10:1 intensity range was about 20% larger than the physical slit width.

Conclusions

The use of small probe to particle diameter ratios in phase Doppler interferometry has been shown to produce accurate droplet size measurements when using a combined phase and intensity validation scheme. Without these validation criteria serious overestimation of the higher moment diameters can occur as a result of droplets being erroneously measured as much larger droplets. It has also been shown that a phase validation criteria using integer values of the detector separation ratio will validate most of the trajectory errors. A non-integer detector separation ratio has been demonstrated to reject large droplets being erroneously reported as much smaller droplets. The phase validation criteria does, however, still validate some small droplets being measured as much larger droplets. The 10:1 intensity validation criteria does reject these errors and provides a very robust and simple method for determining the probe cross-sectional area, which greatly affects mass flux measurements.

The use of small probe volumes can greatly improve measurement reliability in dense sprays, where multiple particle occurrences in the probe volume will affect the measurement.

References

1. S.V. Sankar, D.H. Buermann, A.S. Inenaga, K.M. Ibrahim and W.D. Bachalo, "Coherent Scattering In Phase Doppler Interferometry: Response of Frequency Domain Processors", 7th Intl. Symp. on Appl. of Laser Techniques to Fluid Mechanics, Lisbon, Portugal, July 11-14, 1994.
2. Y. Hardalupas and C. H. Liu, Implications of the Gaussian Intensity Distribution of Laser Beams on the Performance of the Phase Doppler Technique. Sizing Uncertainties", *Prog. Energy Combust. Sci.*, Vol 23, pp. 41-63, 1997.
3. Per Haugen, Edward I. Yates, Hans-Henrik von Benzon, "Size and Velocity Measurements of Large Drops in Air and in a Liquid-Liquid Two-Phase Flow by the Phase-Doppler Technique" (*Part. Part. Syst. Charact.*, Vol. 11, pp. 63-72, 1994. ?
4. Y. Hardalupas and A. M. K. P. Taylor, "Phase Validation Criteria of Size Measurements for the Phase Doppler Technique", *Experiments in Fluids*, Vol. 17, pp. 253-358, 1994.
5. P.A. Strakey, D.G. Talley, W.D. Bachalo and S.V. Sankar, "The Use of Small Probe Volumes with Phase Doppler Interferometry" 11th Annual Conference on Liquid Atomization and Spray Systems, ILASS-Americas '98, Sacramento, CA, May 17-20, 1998.
6. P.A. Strakey, D.G. Talley and W.D. Bachalo, "Phase Doppler Measurements in Dense Sprays" 11th Annual Conference on Liquid Atomization and Spray Systems, ILASS-Americas '98, Sacramento, CA, May 17-20, 1998.
7. S.V. Sankar and W.D. Bachalo, "Response Characteristics of the Phase Doppler Particle Analyzer for Sizing Spherical Particles Larger Than the Light Wavelength", *Applied Optics*, Vol. 30, No. 12, pp. 1487-1496, 20 April 1991
8. Huihe Qui and Chin Tsau Hsu, "Method of phase-Doppler anemometry free from the measurement-volume defect", *Applied Optics*, Vol. 38, No. 13, pp. 2737-2742, May 1, 1999. *Stalico*
9. Gerard Grehan, Gerard Gouesbet, Amir Naqwi and Franz Durst, "Trajectory Ambiguities in Phase Doppler Systems: Study of a Near-Forward and Near-Backward Geometry", *Part. Part. Syst. Charact.*, Vol. 11, pp. 133-144, 1994.
10. A. Naqwi, F. Durst and X.-Z. Liu, "An Extended Phase-Doppler System for Characterization of Multiphase Flows", 5th Intl. Symp. on Appl. of Laser Techniques to Fluid Mech., Lisbon, Portugal, July, 1990.
11. G. Grehan, G. Gouesbet, A. Naqwi and F. Durst, "Trajectory Ambiguities in Phase Doppler Systems: Use of Polarizers and Additional Detectors to Suppress the Effect", 6th Intl. Symp. on Appl. of Laser Techniques to Fluid Mech., Lisbon, Portugal, July, 1994.
12. Y. Aizu, M. Ziemann, X. Liu, S. Hohmann and F. Durst, "PDA System Without Gaussian Beam Defects" 3rd Intl. Congress on Optical Particle Sizing, Yokohama, Japan, August, 1993.
13. C. Tropea, T.-H. Xu, F. Onofri, G. Grehan and P. Haugen, "Dual Mode Phase Doppler Anemometry", 7th Intl. Symp. on Appl. of Laser Techniques to Fluid Mech., Lisbon, Portugal, July, 1994.
14. S. V. Sankar and W. D. Bachalo, "Performance Analysis of Various Phase Doppler Systems", 4th International Congress on Optical Particle Sizing, Nuremberg, Germany, March 21-23, 1995.

15. S.V. Sankar, A.S. Inenaga and W.D. Bachalo, "Trajectory Dependent Scattering in Phase Doppler Interferometry: Minimizing and Eliminating Sizing Errors", *6th Intl. Symp. on Appl. of Laser Techniques to Fluid Mechanics*, Lisbon, Portugal, July 20-24, 1992.
16. S.V. Sankar, W.D. Bachalo and D.A. Robart, "An Adaptive Intensity Validation Technique for Minimizing Trajectory Dependent Scattering Errors in Phase Doppler Interferometry", *4th Intl. Congress on Optical Particle Sizing*, Nuremberg, Germany, March 21-23, 1995.
17. T-H Xu and C Tropea, "Improving the Performance of Two-Component Phase Doppler Anemometers", *Meas. Sci. Technol.*, Vol. 5, pp. 969-975, 1994.

Nomenclature

A	probe cross-sectional area (μm^2)
D	droplet diameter (μm)
D_s	apparent slit width (μm)
D_w	$1/e^2$ beam waist diameter (μm)
$D_{w10\%}$	probe diameter at $1/10^{\text{th}}$ of I_{max} (μm)
D_{10}	number mean diameter (μm)
D_{32}	Sauter mean diameter (μm)
N	droplet number density (cc^{-1})
n	number of droplets in probe volume
S	detector separation (mm)
ϕ	phase difference
η	trajectory coordinate
θ	scattering angle

Subscripts

12	denotes detectors 1 and 2
13	denotes detectors 1 and 3

Table 1 : Configuration for experiments and model calculations.

	Case 1	Case 2
Beam Separation (mm)	21	21
Transmitter Focal Length (mm)	470	470
Receiver Focal Length (mm)	500	500
Scattering Angle (deg)	30	30
Initial Beam Diameter (mm)	10.0	10.0
$1/e^2$ Beam Waist Diameter (μm)	60	60
Slit Width (μm)	50	50
Receiver Magnification	2.0	2.0
Receiver Lens Diameter (mm)	105	105
Laser Wavelength (nm)	514.5	514.5
Fringe Spacing (μm)	11.52	11.52
S_{12} (mm)	23.34	25.0
S_{13} (mm)	69.00	65.0
S_{13}/S_{12}	2.96	2.6
Sample Rate (MHz)	160	160
Sample Size	64	64
Threshold (mv)	3.0	3.0

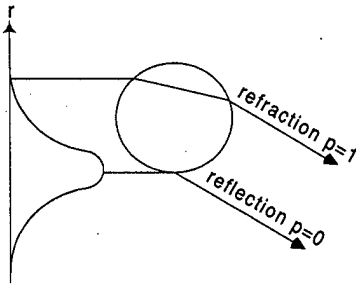


Figure 1: Trajectory dependent scattering.

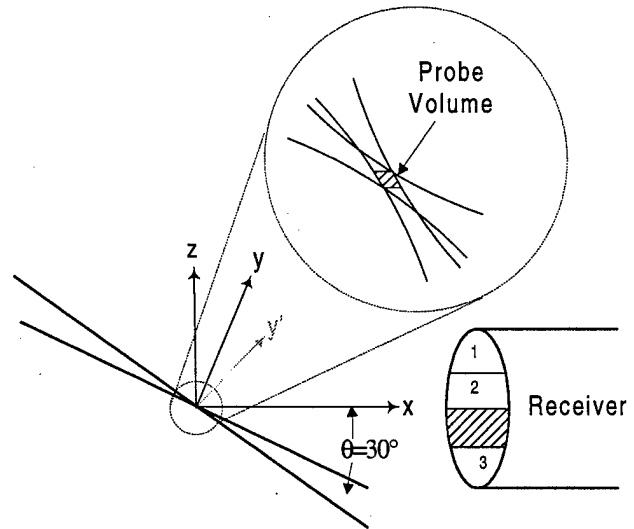


Figure 2: Optical arrangement for modeling calculations.

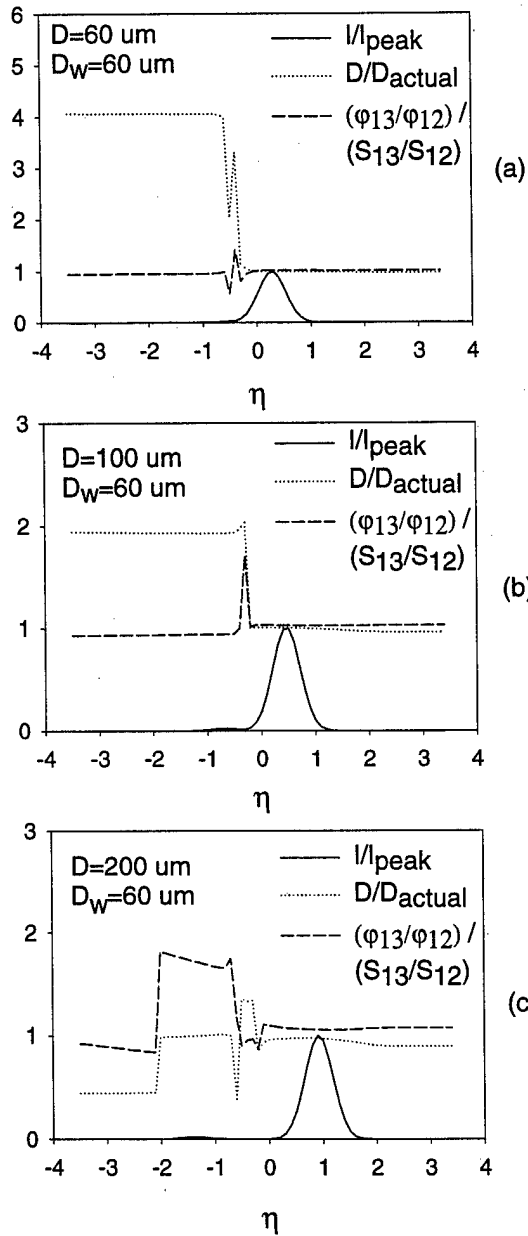


Figure 3: Model calculations of normalized: scattered light intensity, diameter and phase ratio for diameters of (a) 60 μm , (b) 100 μm and (c) 200 μm . Water droplets, optical arrangement of case 1, Table 1.

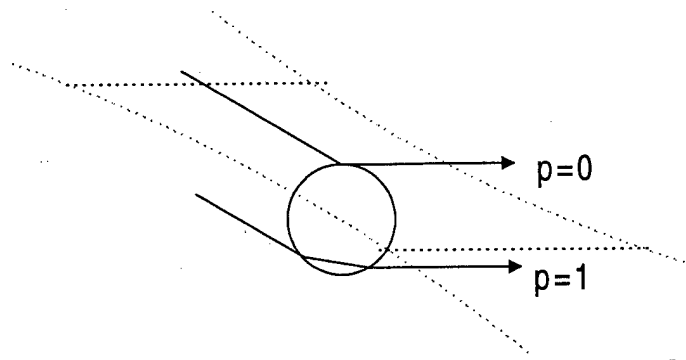


Figure 4: Illustration of slit effect. Dashed lines correspond to beam edge (light dashed line) and slit edge (dark dashed line). Ray paths of reflection ($p=0$) and refraction ($p=1$) are shown.

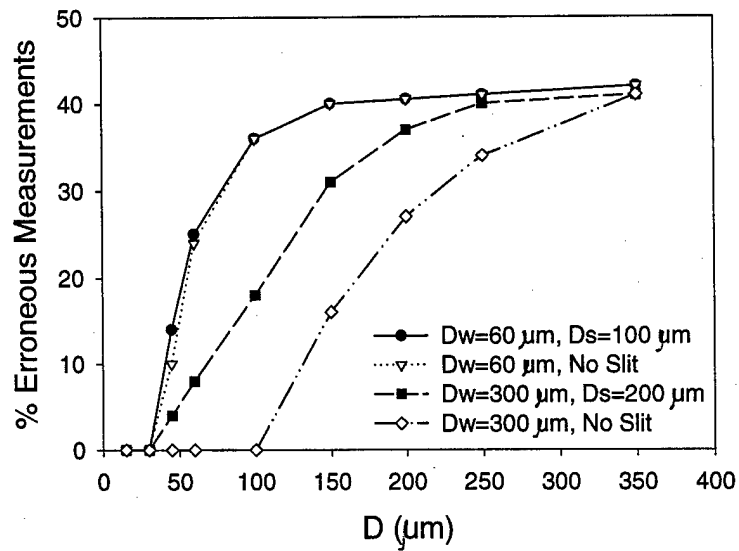


Figure 5: Fraction of measurements with significant sizing errors versus droplet size for $60 \mu\text{m}$ and $300 \mu\text{m}$ probe diameter, with and without slit effect.

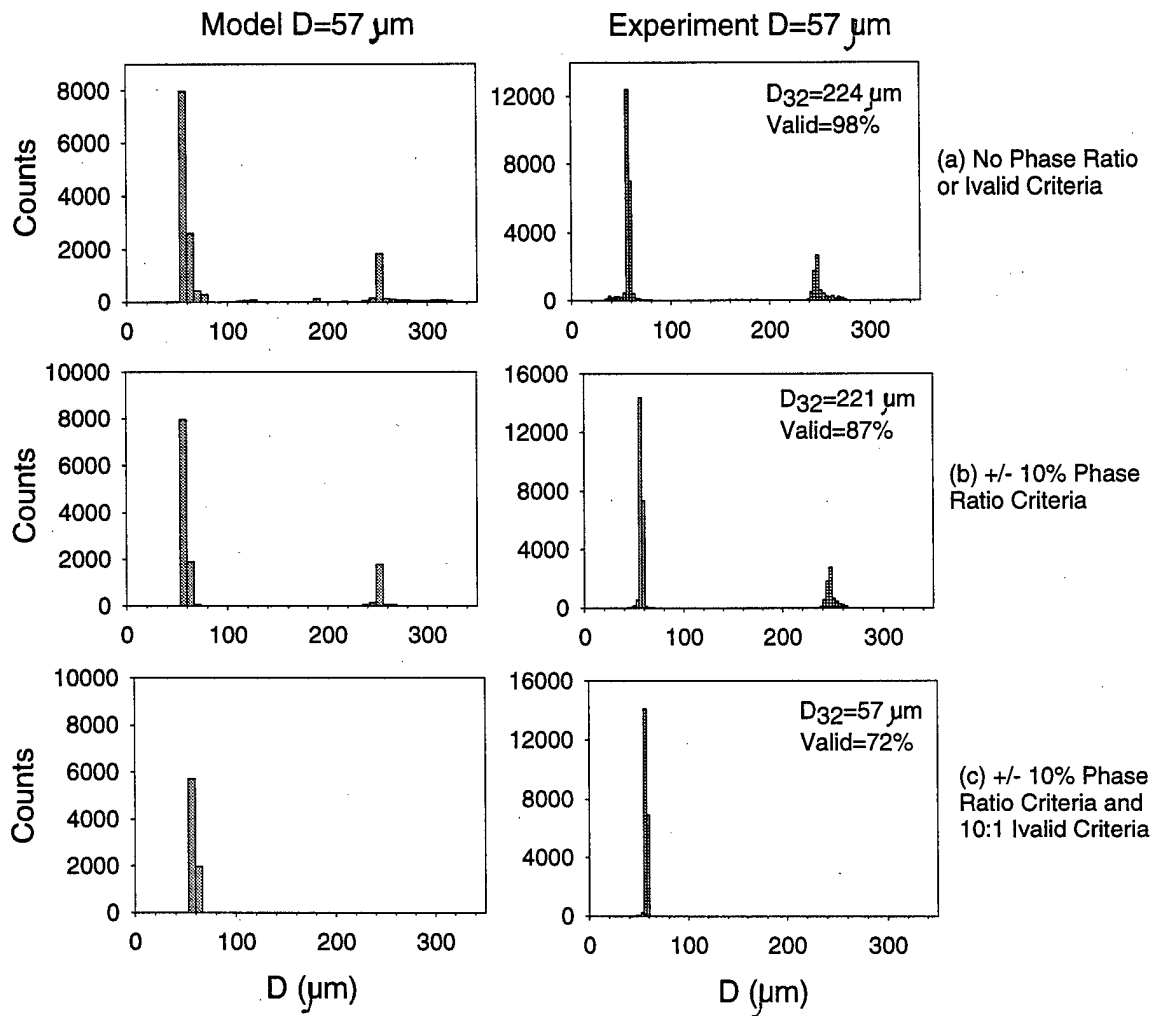


Figure 6: Histograms of calculated droplet size (left series) and measured droplet size (right series) for 57 μm droplets on random trajectories. (a) without phase ratio criteria, (b) with phase ratio criteria and (c) with phase ratio and 10:1 intensity validation criteria. Water droplets, optical configuration from case 1, Table 1.

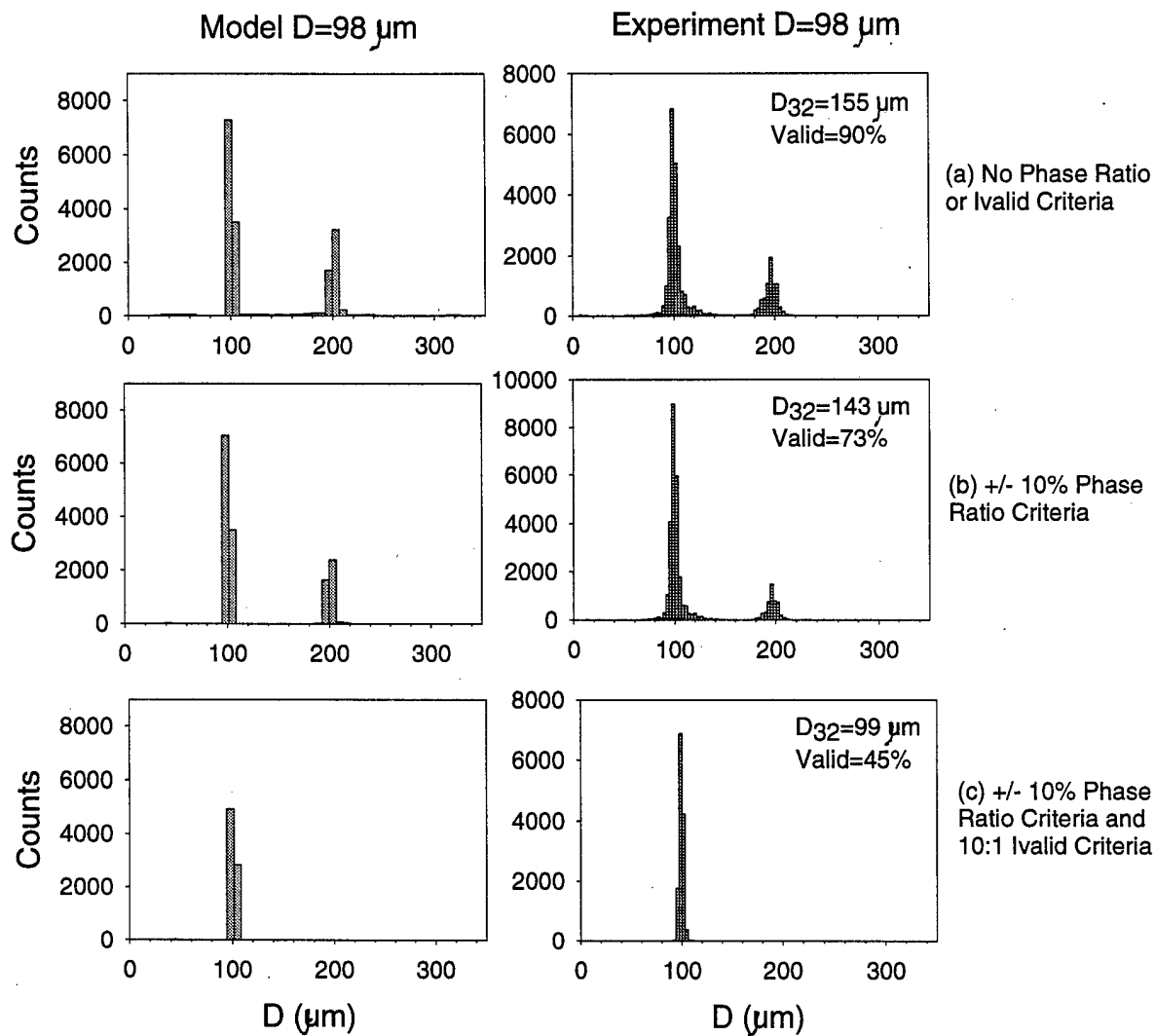


Figure 7: Histograms of calculated droplet size (left series) and measured droplet size (right series) for 98 μm droplets on random trajectories. (a) without phase ratio criteria, (b) with phase ratio criteria and (c) with phase ratio and 10:1 intensity validation criteria. Water droplets, optical configuration from case 1, Table 1.

Experiment $D=250\ \mu\text{m}$

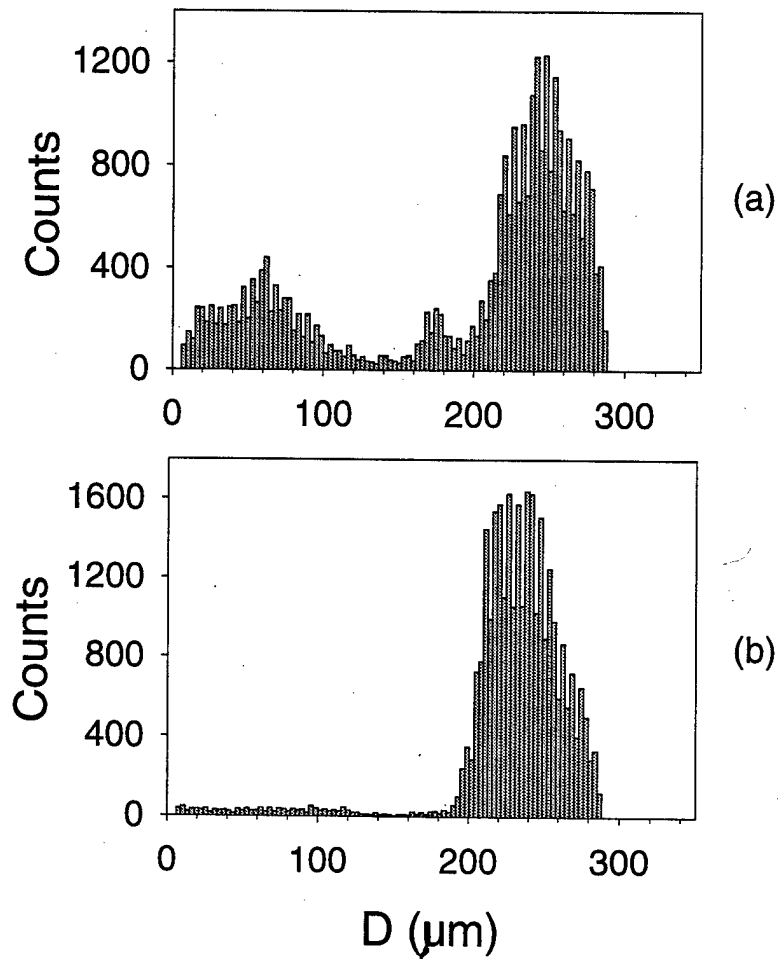


Figure 8: Histograms of measured counts for $250\ \mu\text{m}$ water droplets on random trajectories (a) without phase ratio criteria and (b) with phase ratio criteria. Non-integer detector separation, optical configuration from case 2, Table 1.

Experiment D=61 μm

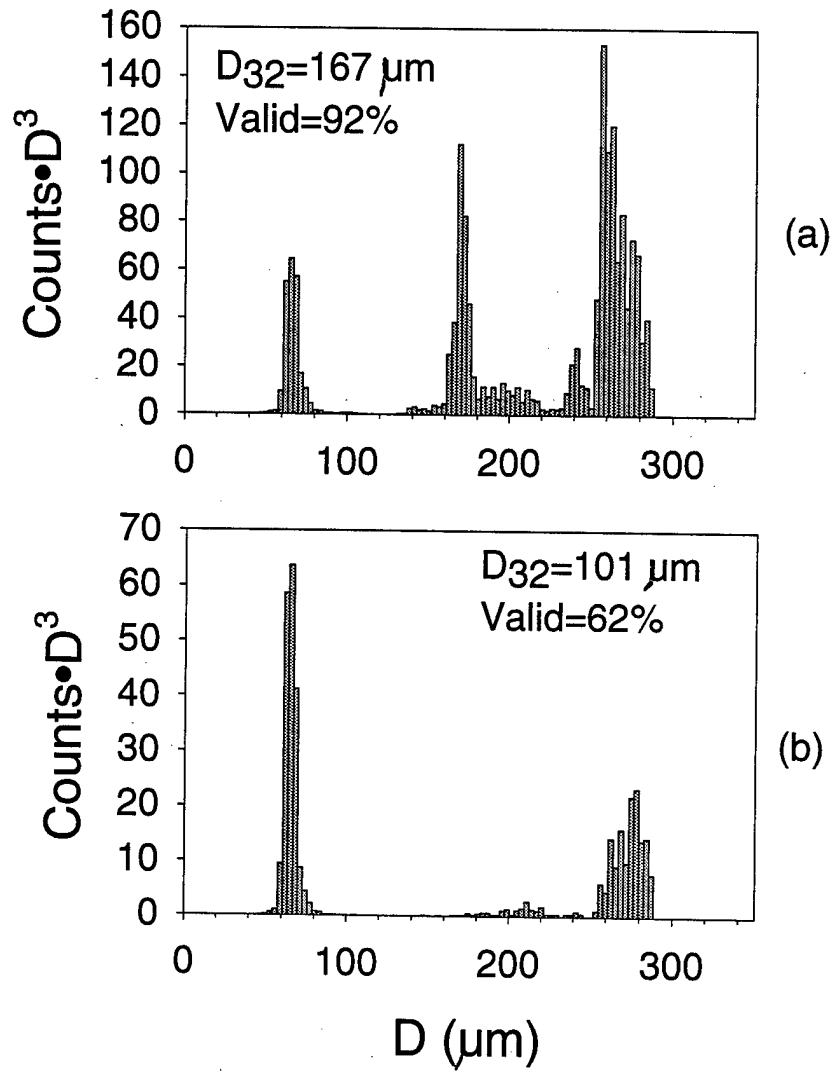


Figure 9: Relative volume distributions (counts $\cdot D^3$) for 61 μm water droplets on random trajectories (a) without phase ratio criteria and (b) with phase ratio criteria. Non-integer detector separation, optical configuration from case 2, Table 1.

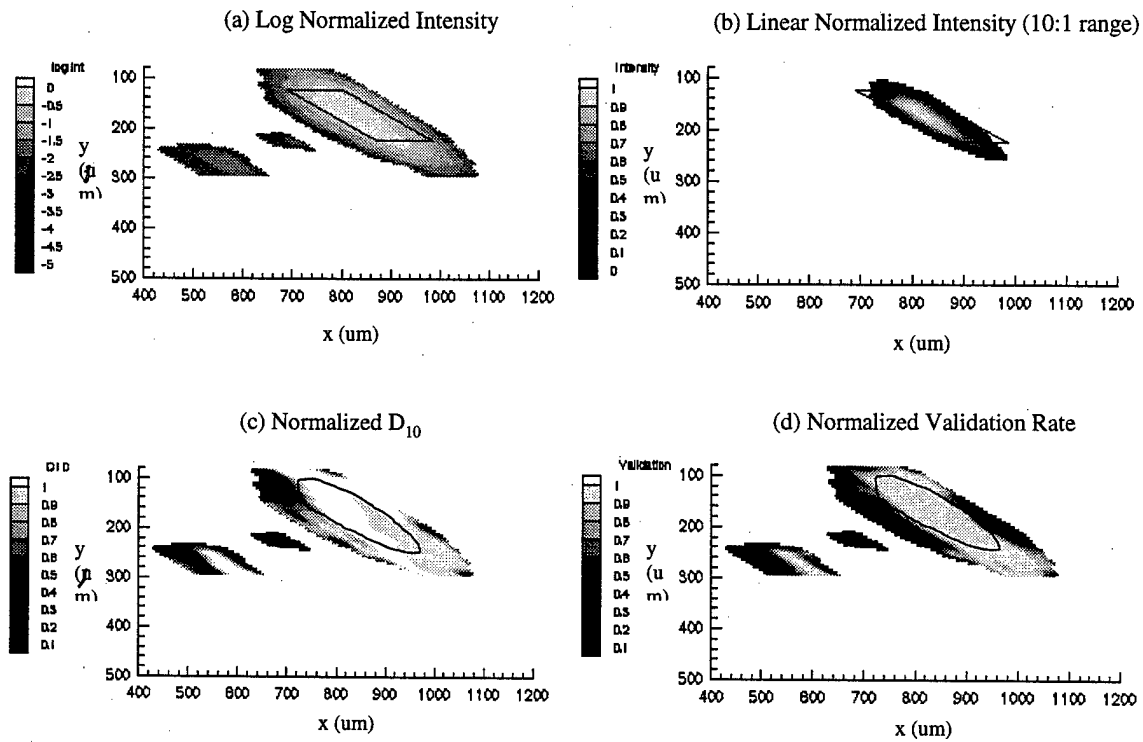


Figure 10: Contour plots of measured (a) log of the normalized intensity, (b) linear normalized intensity over 10:1 range, (c) normalized D_{10} and (d) normalized validation rate. Assumed probe cross-section shown by parallelogram. 330 μm glass bead, optical configuration from case1, Table 1.